Supplementary Information

1. Collagen fiber in tissue slices of breast cancer at different stages

To better illustrate the differences between isotropic and anisotropic arrangement of collagen fibers in the matrix, we employed H&E staining and SHG imaging to stain and observe the morphology of collagen fibers and cancer cells in breast cancer patient tissue slices. As shown in Fig. S1 A1-A3, for early-stage breast cancer, collagen fibers in the slice are isotropic, and cells are disorderly located in the collagen fiber network. In contrast, late-stage breast cancer exhibits a distinct alteration in the arrangement of collagen fibers. As illustrated in Fig. S1 B1-B3, these fibers transition from an isotropic network to anisotropic bundles following collagen deposition, with the tumor cells dispersed among these reorganized fibrous structures. This change indicates the increase in the density of collagen fibers as well as its significant changes with the progression of cancer, which is consistent with the previously observed results.[1-3]
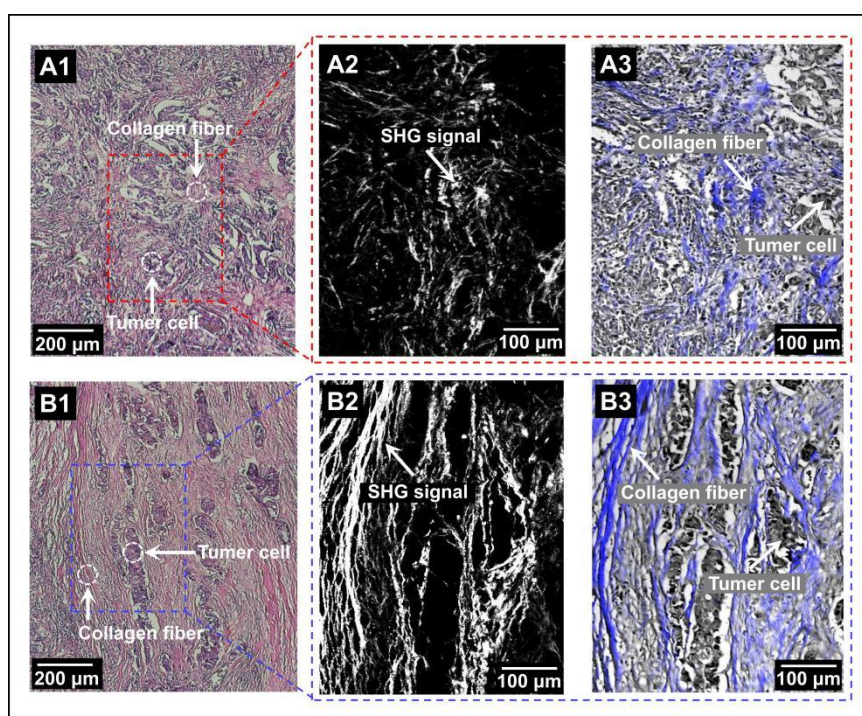
Fig. S1 H&E staining and SHG images of cancer cells and collagen fibers in breast cancer tissue sections at different stages. (A1) and (B1) represent H&E staining images of early-stage and late-stage breast cancer tissue sections, respectively. (A2)-(A3) and (B2)-(B3) are SHG images of collagen fibers and combined images of collagen fibers with cancer cells in local areas of (A1) and (B1), respectively. The images in (B1)-(B3) are referenced as in our group's previous study (Liu et al., Proc. Natl. Acad. Sci. USA, 2016).

2. The design principle of micropillars on chip cover

To demonstrate the functionality of fusiform micropillars on chip cover in forming anisotropic collagen fibers, we performed flow field simulation (in COMSOL Multiphysics 5.6) and experimental verification on the chip containing fusiform, rhombic, and oval micropillars. The Flow Field simulation diagrams (Figs. S2 A1-A3) indicate that the velocity of collagen flow was faster in the fusiform micropillar chip. Our simulation further indicated that, when injecting collagen, bubbles that affected the consistency of the collagen matrix in the chip were more likely to occur in the chips with rhombic and oval micropillar than in chips with fusiform micropillar chips (shown in Figs. S2 B1-B3). Moreover, after the solidification of the collagen solution in the three types of chips, the collagen fibers within the fusiform micropillar chip were more prone to form an anisotropic collagen fiber microenvironment compared to the other two (illustrated in Figs. S2 C1-C3).
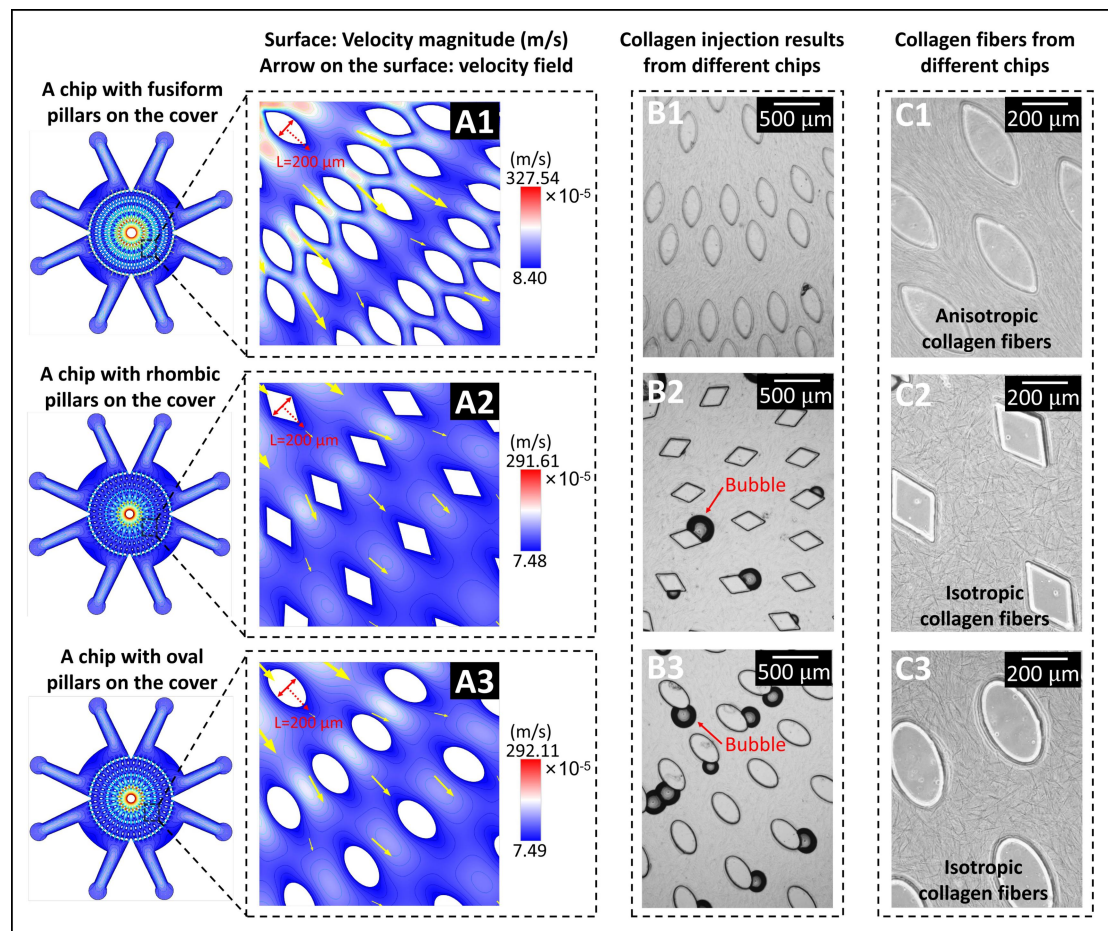
Fig. S2 The design principle of micropillars on chip cover. (A1)-(A3) Flow field simulation diagram of collagen in the chip with fusiform, rhombic, and oval micropillars, respectively. (B1)-(B3) and (C1)-(C3) are situations of bubbles and fibers in curved collagen of chips with fusiform, rhombic, and oval micropillars, respectively.

3. Stereoscopic representation of microchamber implanted with breast cancer cells

To show a more comprehensive structure of the chip microchamber implanted with breast cancer cells, three-dimensional (3D) images of the microchamber were captured by confocal microscopy (SP8, Leica, Germany). Fig. S3 shows the microchamber in the collagen formed as a sealed columnar space, allowing the cells to accumulate and be directly embedded into the collagen. After being injected into chip channels, the medium permeates through the matrix into the microchamber to culture the breast cancer cells. This setup allows the sealed microchamber to serve as a tumor lesion in the experiment, thus making the chip more realistic for simulating the progress of breast cancer.
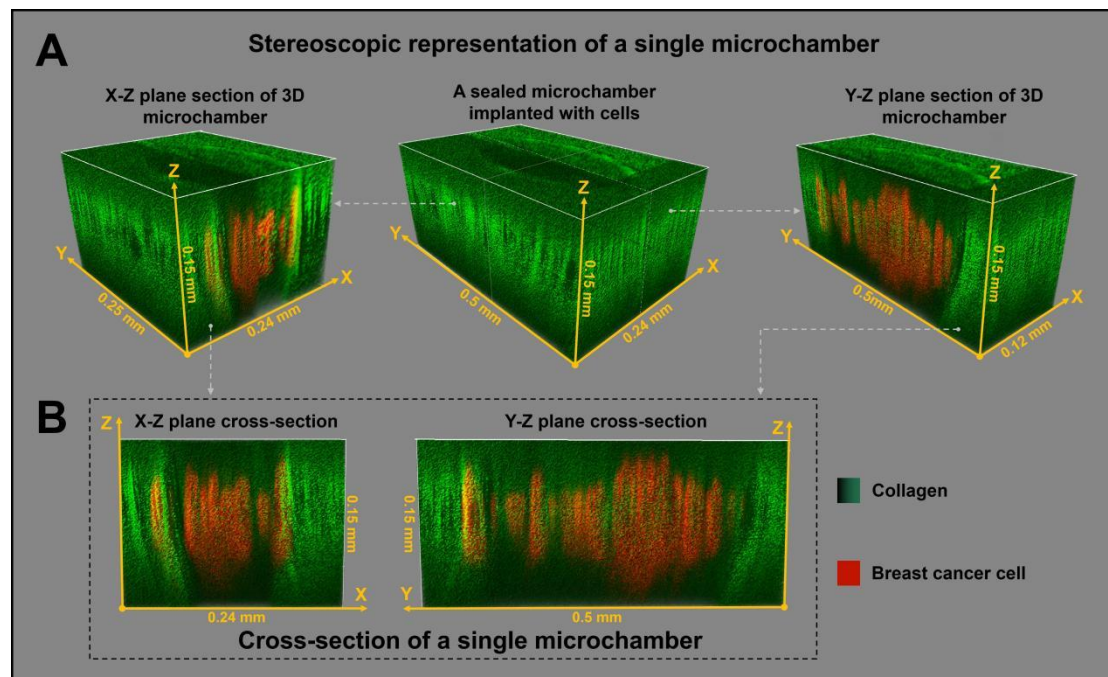
Fig. S3 Stereoscopic representation of microchamber implanted with breast cancer cells. (A) 3D microchamber images from different perspectives. (B) 2D cross-section images of the microchambers from different perspectives.

4. Statistical test for angular frequency standard deviation of isotropic and anisotropic collagen fibers

After constructing the isotropic and anisotropic collagen fiber matrices according to the methods described in Section 2.3, we captured the SHG images of collagen fibers in both matrices using confocal two-photon microscopy. Subsequently, we analyzed the angular

distribution frequency of collagen fibers using the Curvelet-Based Alignment Analysis software (University of Wisconsin at Madison). The results in Fig. 3A5 and B5 indicated that when the angular frequency of collagen fibers was counted with the horizontal direction as the starting angle, the angles of anisotropic collagen fibers were more concentrated around 0°, while those of isotropic collagen fibers were distributed more uniformly between 0° and 180°.

To further compare the differences in collagen fiber arrangement between the two matrices, we calculated the standard deviation (σ) of the angular distribution frequency of collagen fibers in chips of Fig. 3A5 and 3B5. This allowed us to compare the degree of concentration of collagen fiber arrangement angles. A higher standard deviation (σ) of the angular distribution frequency indicates a more concentrated distribution of collagen fiber angles in a particular direction, indicating anisotropy. Through statistical testing of σ across multiple samples, the results are presented in Fig. S4. The mean value of σ for the angular distribution frequency of isotropic collagen fibers was 0.0127, while the mean value of σ for the angular distribution frequency of anisotropic collagen fibers was 0.0384. Analysis of the data using a T-test revealed a significant difference in σ between the two collagen fiber distribution angles (P-value=0.0017). This demonstrates the successful construction of our isotropic and anisotropic collagen fiber matrices.
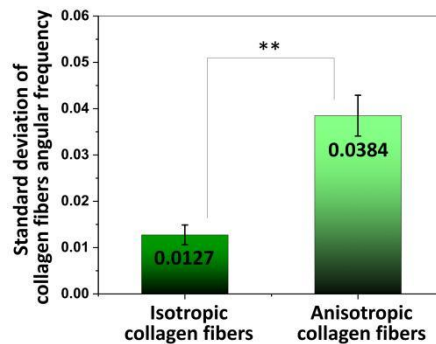
Fig. S4 The significance analysis of angular frequency differences between isotropic and anisotropic collagen fibers in chips. Standard deviations of angular frequencies of collagen fibers were calculated separately in three isotropic and anisotropic chips to assess the degree of concentration in the alignment of collagen fibers. A higher standard deviation value indicates a more uniform alignment of collagen fibers and a more prominent anisotropic characteristic. A t-test was employed to analyze the significance of differences in the standard deviations of angular distribution between isotropic and anisotropic collagen fibers, revealing a significant difference with a P-value of 0.0017. $^{ns}P > 0.05$, $^{*}p < 0.05$, $^{**}p < 0.01$, $^{***}p < 0.001$.

5. Reliability test of cell number characterization method

There is a high correlation between Red Fluorescent Protein (RFP) fluorescence intensity and cell number. To verify such with the RFP fluorescence signal of MDA-MB-231-RFP cells in our experiment, we used Ki67 for immunofluorescence assay to analyze the fluorescence signal similarity between RFP and Ki67 of cells in the chip (The Ki67 protein is highly associated with cancer cell mitosis and is often used in cancer cell characterization[4-6]).

We took from the jigs the chips without drug at different time stages and removed the residual medium. We then rinsed the ECM region with 400.0 ul preheated 1×PBS (from Corning, NY, USA) three times and used 400.0 ul preheated 4.0% paraformaldehyde (Beyotime, China) to soak the ECM region for 1.0 h to fix the cells. After removing the 4.0% paraformaldehyde, we again rinsed the chips with 1×PBS. 400.0 ul normal goat serum (Solarbio, China) was then used to incubate the chip at 37.0℃ for 3.0 h, and the chip pretreatment was finished with complete removal of the serum.

For the labeling of Ki67, we diluted the primary antibody Anti-Ki67 Rabbit pAb (GB111499, Servicebio, China) in 1×PBS at a ratio of 1:1000. We employed 200.0 ul of diluent to incubate the chip in the dark at 4.0℃ for 12.0 h. After that, the chips were rinsed with 1×PBS three times to remove any remaining Ki67 primary antibodies. Then, we diluted the secondary antibody Ki67 FITC conjugated Goat Anti-Rabbit lgG (H+L) (GB22303, Servicebio, China) with 1×PBS at the ratio of 1:200, and we used 200.0 ul of diluent to incubate the chip at 37.0℃ in dark for 3.0 h. Following the removal of the secondary antibody, we washed the chips with 1×PBS to complete the labeling of Ki67. To assist with labeling the nucleus, we employed 200.0 μl DAPI dye solution (C1005, Beyotime Biotechnology, China) for incubating the chip at room temperature in the dark for 10.0 min. Then, 30.0 ul antifading (S2100, Solarbio, China) was used to seal the chip. Finally, images of the Ki67, RFP, and DAPI in cells were captured with confocal microscopy (SP8, Leica, Germany).

As shown in Fig. S5 A1-A3, fluorescence images of RFP, Ki67, and DAPI of breast cancer cells in the Ki67 staining experiment of 24.0 h exhibited significant similarity in the number and location of fluorescence signal points. We used a Python program to refine our calculation further and to analyze the cosine similarity between the Ki67, DAPI, and RFP fluorescence signal images (cosine similarity is a tool widely used for image similarity and biological data

analysis).[7,8] More precisely, we divided the images into eight rectangular regions and compared the number of fluorescent signal points in eight regions of every two images (the results shown in Figs. S5 B1-B2). In both isotropic and anisotropic matrices, the similarities of three fluorescence signals are higher than 90.00% during the culture process from 24.0 h to 120.0 h, indicating that the RFP fluorescence signal in our experiment is very similar to the Ki67 and DAPI fluorescence signals. Thus, the RFP fluorescence intensity can reliably characterize the number of MDA-MB-231-RFP cells in the experiment.
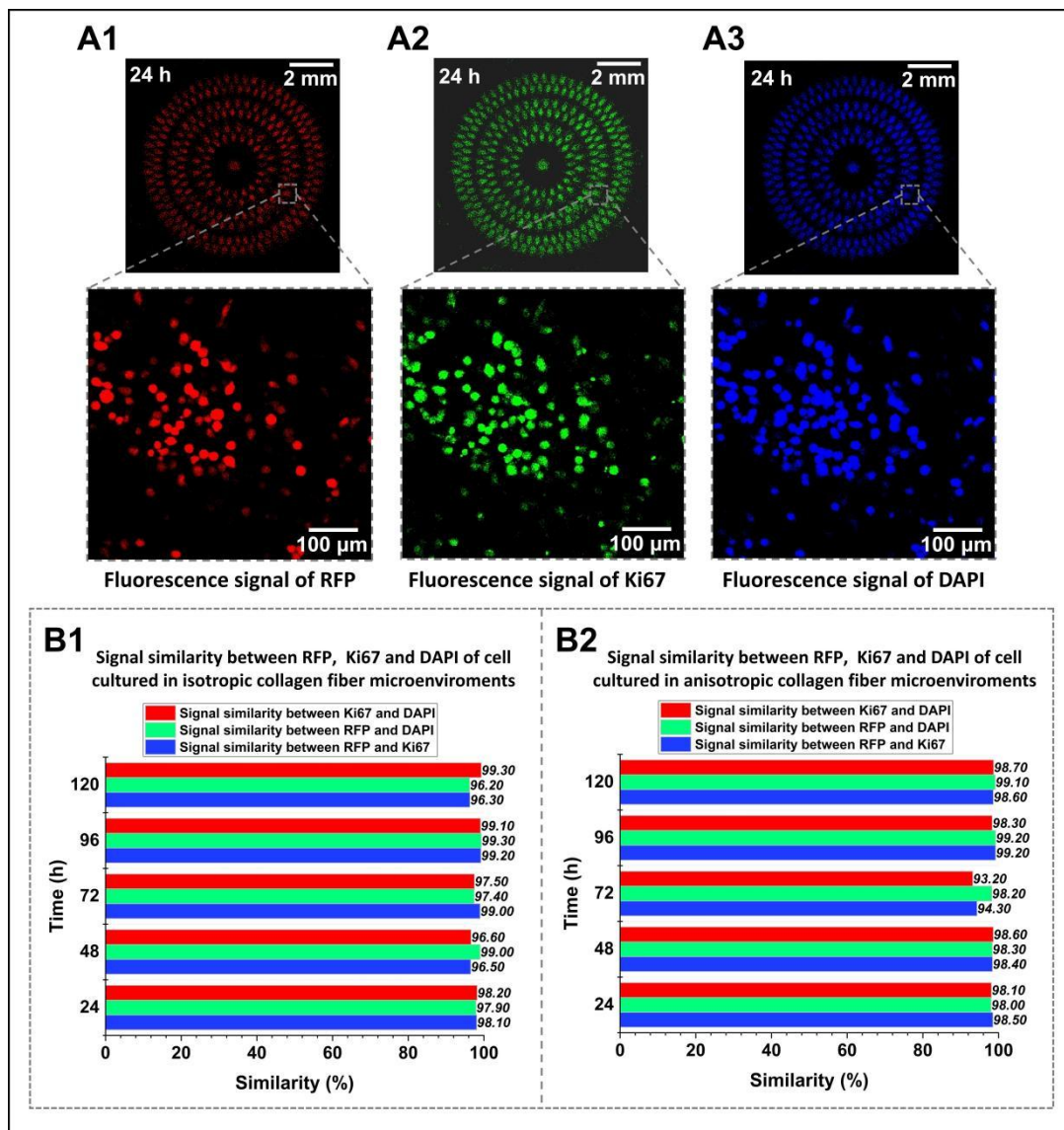
Fig. S5 Ki67 staining experimental results for reliability test of the cell number characterization method. (A1)-(A3) RFP, Ki67, and DAPI fluorescence images of breast cancer cells cultured in isotropic collagen fiber microenvironment without drug for 24.0 h. (B1)-(B2) Similarity analysis of RFP, Ki67, and DAPI fluorescence images of breast cancer cells cultured in isotropic and anisotropic collagen fiber microenvironments without drugs from different stages.

6. Analysis method of cell fluorescence intensity in Figs. 5 B1-B4 and Figs. 6 B1-B4

In Figs. 5 B1-B4 and Figs. 6 B1-B4 of our manuscript, the dynamic fluorescence intensity changes of MDA-MB-231-RFP cells at different times and space were plotted to assess the cell number indirectly. We divided the cell fluorescence images into 20 rows and 20 columns to obtain 400 sub-regions of equal size and then analyzed the fluorescence intensities using MATLAB. The fluorescence intensity of cells in a specific sub-region *n* and time *t* is represented by *I (n, t)*, where *n* = 0, 1, … 400, and *t* = 0, 24.0, … 120.0 h. Then, to present the comprehensive dynamics of cell behaviors, including proliferation and migration within a sub-region at different time points, the cell fluorescence intensity rate *R (n, t)* is employed and defined by the following equation:

$$\mathbf{R}(\boldsymbol{n}, \boldsymbol{t}) = \frac{\mathbf{I}(n,t)}{\mathbf{I}(n,0)} \tag{1}$$

where *I (n, 0)* is the fluorescence intensity of cells in sub-region *n* at 0 h, and *I (n, t)* is the fluorescence intensity of cells in sub-region *n* at *t* h.

7. Analysis method of specific growth rate in Figs. 5 C1-C2 and Figs. 6 C1-C2

We used the statistical method of sub-regional analysis to compare and analyze the effects of different drugs on cell proliferation and migration. As shown in Figs. 5 C1-C2 and Figs. 6 C1-C2 of manuscript, the ECM region was divided into 16 sub-regions, and each sub-region was divided into five smaller areas named *a*, *b*, *c*, *d*, *e*. We then calculated the cell growth rate using the following statistical formula for cell division:

$$\frac{\mathbf{dN}}{\mathbf{dt}} = \mu \mathbf{N} \tag{2}$$

At any time (*t*), the growth rate of cell number (*dN/dt*) is proportional to the total number of original cells (*N*). After integration and deformation, we obtain:

$$\mu = \frac{1}{t}\ln\left(\frac{\mathbf{N_t}}{\mathbf{N_0}}\right) \tag{3}$$

In this formula, *t* is any time, *N₀* is the initial number of cells, *Nₜ* is the number of cells at time *t*, and *μ* is the specific growth rate.

Cell numbers were considered to be proportional to the cell fluorescence intensity for these measurements, as proved as a effective indicator in previous researches.[12, 13] From here, for an indirect assessment of cell number, we computed the dynamic fluorescence

intensity changes of MDA-MB-231-RFP cells over varying time and space. In our experiment, the cell number (N_t, N_0) was replaced by the cell fluorescence intensity (I_t, I_0). The growth rate of fluorescence intensity per unit area i can then be calculated using:

$$\mu_i = \frac{1}{t}\ln\left(\frac{I_t}{I_0}\right) \tag{4}$$

The chips shown in Fig. 5 C1 and Fig. 6 C1 were divided into 16 fan-shaped regions marked 1-16, respectively. Fig. 5 C3 and Fig. 6 C3 presented the specific growth rates of these regions. To improve the precision of calculating the fluorescence intensity of each data point, each segment was further subdivided into five smaller fan-shaped regions labeled *a, b, c, d*, and *e*. Then, by integrating this result, the average specific growth rate of fluorescence intensity of multiple unit areas i in the region *a* was calculated as:

$$\mu_a = \frac{1}{\int_0^{\frac{\pi}{40}} \int_0^r r\,dr\,d\theta} \sum_1^N \mu_i\,\Delta s_i \tag{5}$$

where *N* is the total number of unit areas*, and* ΔS is the acreage of areas i. Therefore, by calculating the average value of *a, b, c, d*, *e*, the specific growth rate of 1/16 chip was finally obtained:

$$\bar{\mu} = \frac{1}{5}(\mu_a + \mu_b + \mu_c + \mu_d + \mu_e) \tag{6}$$

Lastly, we plotted the specific growth rate of cells in 16 sub-regions under the conditions of isotropic and anisotropic collagen fibers, with and without drugs, at 120.0 h (See Fig. 5 C3 and Fig. 6 C3 of manuscript).

8. Statistical tests on the specific growth rates of cells within and outside the microcavities in isotropic and anisotropic collagen fibers

After analyzing the data on the specific growth rates of cells within and outside the microchambers in isotropic and anisotropic collagen fibers(Fig. 5C3 and Fig. 6C3), statistical tests were conducted on the cell-specific growth rate data corresponding to the 80 small fan-shaped regions within the chips (as demonstrated by the analytical method in Fig. 5C and Fig. 6C, each chip is divided into 16 data regions, with each region containing 5 data units). These tests aimed to assess the statistical significance of differences in cell-specific growth rates across four experimental conditions: isotropic/anisotropic collagen fibers with/without drug treatment. The results of these analyses are presented in Figs. S6 A-B, clearly demonstrating that all p-values are less than 0.001. This indicates the existence of significant

differences in cell-specific growth rates under the aforementioned four experimental conditions.
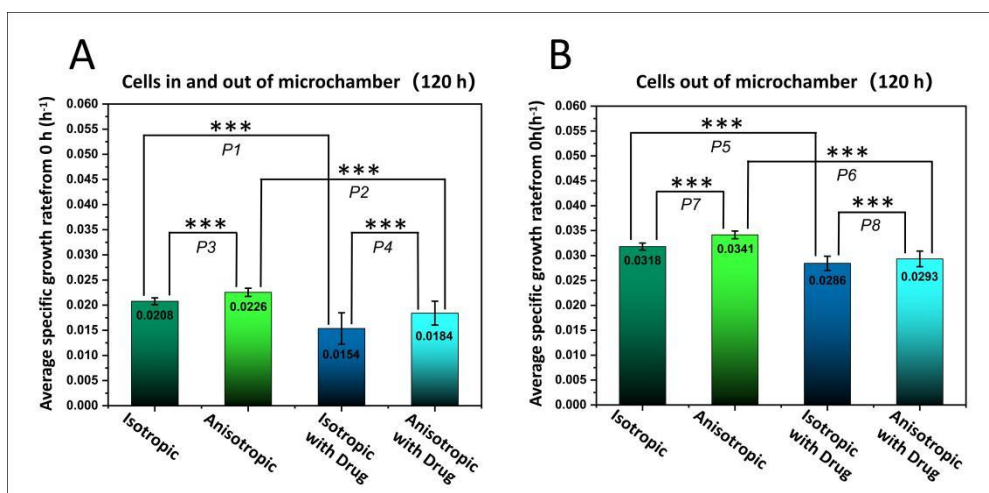
Fig. S6 Statistical analysis of data in Fig.5C3, Fig.6C3, Table 1 and Table 2. (A) Significance analysis of the specific growth rate data for cell proliferation in the entire region of chip was conducted, yielding P-values of P1=1.2290×10^{-32}, P2=1.8410×10^{-31}, P3=2.6151×10^{-32}, and P4=8.9813×10^{-11}. Since all P-values are less than 0.001, the experimental data demonstrates significant differences. (B) Significance analysis of the specific growth rate data for cells out of microchamber revealed the following P-values: P5=1.3178×10^{-41}, P6=2.7328×10^{-56}, P7=3.3926×10^{-45}, and P8=2.8937×10^{-4}. Since all P-values are less than 0.001, the experimental data exhibits significant differences. $^{ns}P > 0.05$, $*p < 0.05$, $**p < 0.01$, $***p < 0.001$.

9. Immunofluorescence for drug targets blocking time

Immunofluorescence was used to study the onset time of drugs in our study for its viability of detecting the expression of cellular proteins. Specifically, we implanted the MDA-MB-231-RFP cells into the chips and cultured them with drugs, following the methods in section 2 of the manuscript. According to our previous dye gradient experiments (in section 3.3 of the manuscript), the concentration gradient took at least 24.0 h to form and stabilize. We conducted immunofluorescence experiments to characterize cells cultured for 24.0 h (see Fig. S7). The fluorescence intensity of cells in the anisotropic matrix was brighter than in the isotropic matrix (shown in Figs. S7 A1 and B1). Notably, the relative expression levels of DDR1 and E-cad were affected near the 7rh and PP2 channels in both isotropic and anisotropic collagen fiber microenvironments (shown in Figs. S7 A2-A3 and B2-B3).
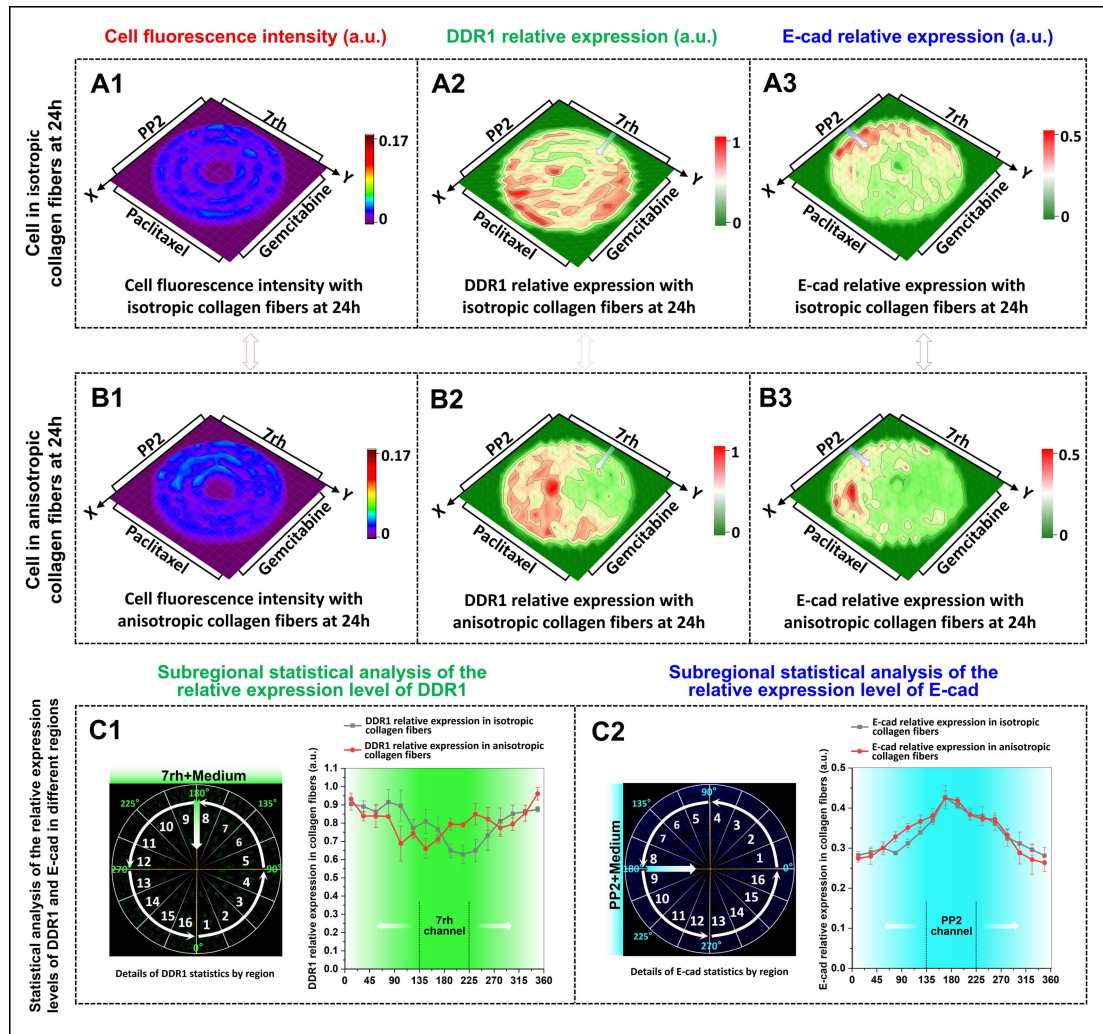
Fig. S7 DDR1 and E-cad expression of MDA-MB-231-RFP cells cultured in isotropic and anisotropic collagen fiber microenvironments for 24.0 h. (A1)-(A3) show fluorescence intensities of RFP and the relative expression of DDR1 and E-cad in isotropic collagen fibers, respectively. (B1)-(B3) show the fluorescence intensities of RFP, as well as the relative expression of DDR1 and E-cad in anisotropic collagen fibers, respectively. (C1)-(C2) showed the subregional statistical analysis of the relative expression levels of DDR1 and E-cad in isotropic and anisotropic collagen fibers at 24.0 h. At 24.0 h, DDR1 expression decreased near 7rh channel and E-cad expression increased near PP2 channel.

Furthermore, to more quantitatively analyze whether 7rh effectively blocked DDR1 in both isotropic and anisotropic matrices, as shown in Fig. S7, we conducted a quantitative statistical analysis of the regional distribution of protein relative expression levels within the microarray in Fig. S7. The results, as presented in Fig. S7C1, indicated that the relative expression level of DDR1 protein in cells was lower between angles 135°-225° corresponding to the 7rh channel compared to other regions. Additionally, as shown in Fig. S7C2, the relative expression level of E-cad protein in cells was higher between angles 135°-225°

corresponding to the PP2 channel compared to other regions. Therefore, these results suggest that in our experiment, the onset time of 7rh and PP2 was approximately 24.0 hours, confirming that cells began to block drug targets shortly after exposure to the drugs. These results were similar to the onset time of the 7rh, and PP2 observed in other previous research.[7-11]

10. Immunofluorescence experiments performed in chip without drug

Immunofluorescence labeling in the chip without any drugs is an important control for assessing the changes in breast cancer cell biology and phenotype under the drug scheme. According to the method in section 2.4, we performed immunofluorescence experiments on cells cultured only in the medium for 120.0 h (results shown in Fig. S6). Regarding RFP fluorescence signals of cells, the intensity in the anisotropic matrix was brighter than that in the isotropic matrix (shown in Figs. S6 A1 and B1), matching the difference in Fig.7 B1 and C1 of the manuscript. More importantly, DDR1 and E-cad in two chip types with anisotropic and isotropic collagen fibers were uniformly expressed in the chip *without* drugs (shown in Figs. S6 A2-A3 and B2-B3). Compared with the chips employed *with* drugs (shown in Fig. 7 B2-B3 and C2-C3 of the manuscript), DDR1 expression turned out higher in the chips without drugs, and E-cad expression was lower. These results proved the inhibitory effect of 7rh on DDR1 expression and the promotion effect of PP2 on E-cad expression, as shown in Fig. 7 of the manuscript.

In general, the expression levels of both DDR1 and E-cad proteins in both chip types without drug were uniform, indicating that our chip can analyze the effects of drug concentration gradients on cells in different regions of the chip, providing a critical control in a specific analysis.
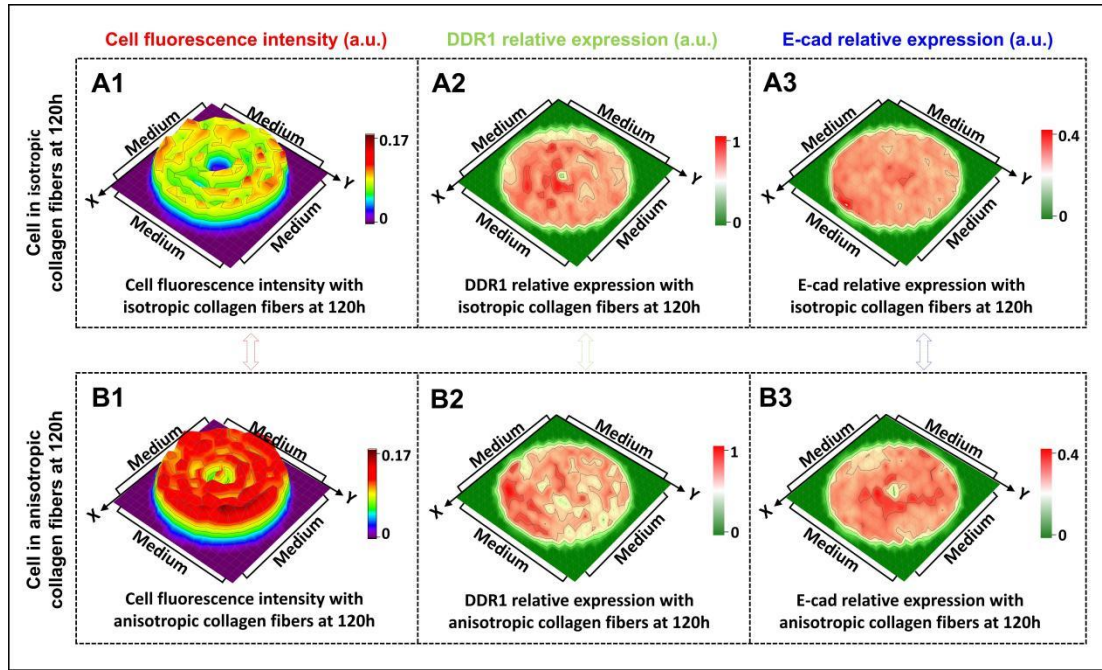
Fig. S8 DDR1 and E-cad relative expression of MDA-MB-231-RFP cells cultured with medium without drugs in isotropic and anisotropic collagen fiber microenvironments for 120.0 h. (A1)-(A3) show fluorescence intensities of RFP and the relative expression of DDR1 and E-cad in isotropic collagen fibers, respectively. (B1)-(B3) show the fluorescence intensities of RFP and the relative expression of DDR1 and E-cad in anisotropic collagen fibers, respectively.

11. Relationship between cell viability and medium channel distance in chip

To validate that cell viability within the chip remains unaffected by the distance from the media channels and to ensure the accuracy of drug response readings, our team employed the Calcein Cell Viability Assay Kit (C2015M, Beyotime Biotechnology, China) and DAPI Staining Kit (G1012, Servicebio, China), following the manufacturer's instructions, to stain both viable and total cell populations within the chip. Specifically, after a 120.0-hour incubation period, chips with cells were detached from the jigs and subsequently stained with Calcein AM + DAPI staining solution, adhering strictly to the protocol, to visualize live cells and the entire cellular constituency. Subsequently, confocal microscopy (SP8, Leica, Germany) was utilized to capture fluorescent images of viable cells and DAPI-stained nuclei within the chip.

For further analysis, six distinct cell seeding regions were delineated, located at distances of 0.7mm, 1.3mm, 1.8mm, 2.5mm, 3.1mm, and 3.7mm from the media channels (Fig. S9A, lef). Utilizing Python (version 3.8), we precisely quantified the number of fluorescent signal

spots corresponding to viable cells and total cells within these designated regions (Fig. S9A, right). The proportion of viable cells (green fluorescent signal spots) to total cells (blue fluorescent signal spots) was calculated and the results are summarized in Fig. S9B. Notably, the ratio of viable cells to total cells remained virtually identical across all distances from the media channels, indicating that cell viability within the chip is largely unaffected by the proximity to the channels. This observation validates that the distance from the media channels does not influence cell viability within the chip, thereby ensuring the accuracy of our experimental drug response readings. Additionally, as shown in Fig. S9C, statistical analysis was conducted on the proportion of viable cells in both substrates, revealing no significant difference. This suggests that the impact of channel distance on viable cell proportion is comparable in both substrates, laying a solid foundation for investigating the differences in drug efficacy between the two chip substrates.
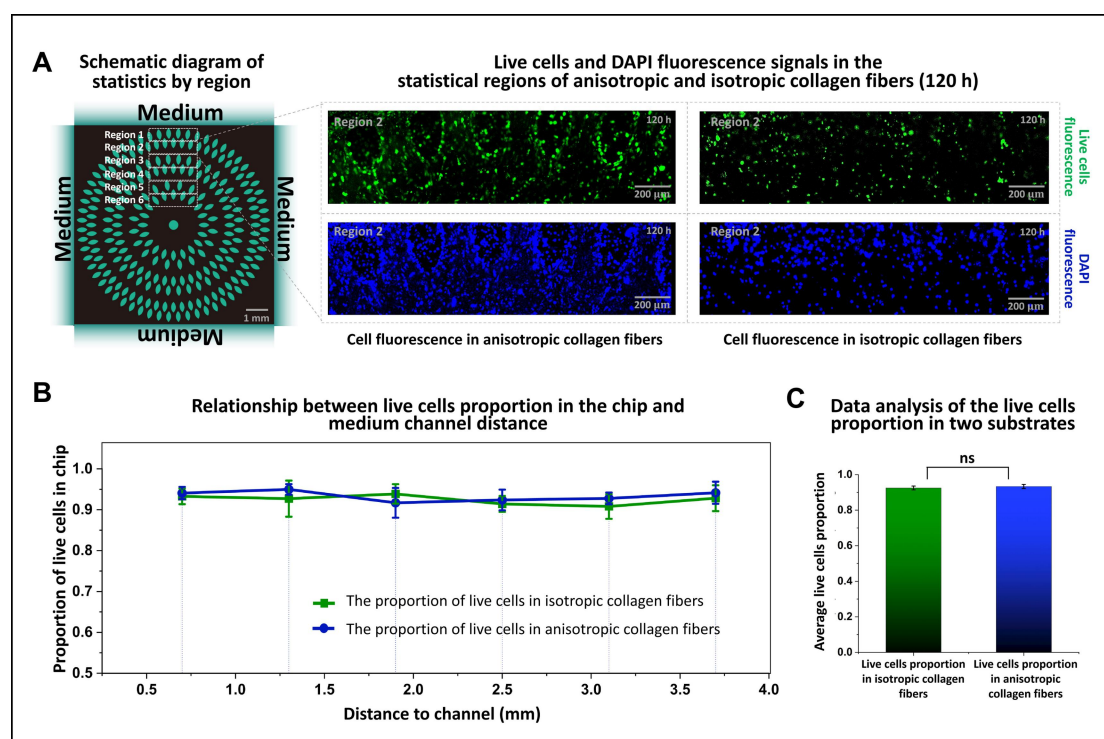
Fig. S9 Test on the relationship between cell viability and medium channel distance in the chip. (A) Regional statistical diagram (left); Live cells and DAPI fluorescence signal in anisotropic and isotropic collagen fibers statistical area at 120.0 h (right). (B) The relationship between the live cells proportion in all cells and medium channel distance in each chip. In isotropic and anisotropic substrates, the proportion of live cells at different distances from the channel is almost the same, and the cell activity in the chip is almost unaffected by the channel distance. (C) Data analysis of the live cells proportion in isotropic collagen fibers and anisotropic collagen fibers. P-value(0.2439)>0.05, there was no significant difference in the proportion of living cells between the two substrates; ^{ns}P>0.05, *p < 0.05, **p < 0.01, ***p < 0.001.

Reference

1. J. N. Ouellette, C. R. Drifka, K. B. Pointer, Y. M. Liu, T. J. Lieberthal, W. J. Kao, J. S. Kuo, A. G. Loeffler and K. W. Eliceiri, *Bioengineering-Basel*, 2021, **8**.

2. L. A. Tomko, R. C. Hill, A. Barrett, J. M. Szulczewski, M. W. Conklin, K. W. Eliceiri, P. J. Keely, K. C. Hansen and S. M. Ponik, *Scientific Reports*, 2018, **8**, 12941.

3. X. Gong, J. Kulwatno and K. L. Mills, *Acta Biomaterialia*, 2020, **108**, 128-141.

4. L. T. Li, G. Jiang, Q. Chen and J. N. Zheng, *Molecular Medicine Reports*, 2015, **11**, 1566-1572.

5. S. S. Menon, C. Guruvayoorappan, K. M. Sakthivel and R. R. Rasmi, *Clinica Chimica Acta*, 2019, **491**, 39-45.

6. M. Juríková, L. Danihel, S. Polák and I. Varga, *Acta Histochemica*, 2016, **118**, 544-552.

7. K. Y. Aguilera, H. C. Huang, W. T. Du, M. M. Hagopian, Z. Wang, S. Hinz, T. H. Hwang, H. M. Wang, J. B. Fleming, D. H. Castrillon, X. M. Ren, K. Ding and R. A. Brekken, *Molecular Cancer Therapeutics*, 2017, **16**, 2473-2485.

8. M. S. Gao, L. Duan, J. F. Luo, L. W. Zhang, X. Y. Lu, Y. Zhang, Z. Zhang, Z. C. Tu, Y. Xu, X. M. Ren and K. Ding, *Journal of Medicinal Chemistry*, 2013, **56**, 3281-3295.

9. Q. P. Lu, W. D. Chen, J. R. Peng, Y. D. Xu, Q. Cai, G. K. Feng, K. Ding, X. F. Zhu and Z. Guan, *Oncology Letters*, 2016, **12**, 3598-3608.

10. J. S. Nam, Y. Ino, M. Sakamoto and S. Hirohashi, *Clinical Cancer Research*, 2002, **8**, 2430-2436.

11. M. P. Sanchez-Bailon, A. Calcabrini, D. Gomez-Dominguez, B. Morte, E. Martin-Forero, G. Gomez-Lopez, A. Molinari, K. U. Wagner and J. Martin-Perez, *Cellular Signalling*, 2012, **24**, 1276-1286.

12. A. Krtolica, C. O. de Solorzano, S. Lockett and J. Campisi, *Cytometry*, 2002, **49**, 73-82.

13. T. A. McCaffrey, L. A. Agarwal and B. B. Weksler, *In Vitro Cellular & Developmental Biology*, 1988, **24**, 247-252.